2023 IEEE International Conference on Autonomic Computing and Self-Organizing Systems (ACSOS) | 979-8-3503-3744-0/23/$31.00 ©2023 IEEE | DOI: 10.1109/ACSOS58161.2023.00034

Radii of Emergent Patterns in Swarmalator Systems

Udo Schilcher, Christoph W. Rauter, and Christian Bettstetter
University of Klagenfurt, Institute of Networked and Embedded Systems, Austria
email: udo.schilcher@aau.at

***Abstract*—For a system of swarmalators converging to different types of circular patterns, we provide expressions for the outer and inner radii of these patterns and examine their dependence on the model parameters. Derivations are made for three static patterns with an infinite number of entities and a generalized swarmalator model with parameterized attraction and repulsion kernels. Simulations of finite systems show good agreement with the asymptotic expressions.**

***Index Terms*—Swarmalators, swarming, synchronization, emergence, self-organizing systems, swarm robotics**

1. Introduction

The theory of swarmalators [1] is an exciting approach for coordination in multi-agent systems. It fuses coordination in space (swarming) and coordination in time (synchronization) into a unified model. Its special feature is the coupling between spatial and temporal coordination: swarming influences synchronization and vice versa. This leads to five types of space-time patterns that emerge depending on the model parameters (see Fig. 1). Applications can be found in biology [2], robotics [3], and other disciplines [4], [5].

Swarmalators can be regarded as a self-organized system, where interactions between entities lead to the emergence of a global pattern [6]. We address a link between the model (microscopic level) and the pattern (macroscopic level) by analyzing the size of the pattern as a function of some model parameters. The model itself reveals no information about the pattern size, not even its order of magnitude. If we want to use the model in practice, an equation or approximation should be helpful in the parameterization.

Section 2 extends the swarmalator model to allow for parameterized kernels. Section 3 derives expressions for the outer and inner radii of the three *static* patterns (Figs. 1a–c) under the assumption that the number of entities approaches infinity. Section 4 compares these asymptotic expressions to simulations with a finite number of entities, showing good agreement in most cases, and analyzes how the radii depend on this number. As a byproduct, we gain insight into the transitions between patterns and reveal two new patterns.

2. System Model

The system consists of $N \in \mathbb{N}$ entities. An entity $i = 1, \dots, N$ is located at point $\boldsymbol{x}_i(t) \in \mathbb{R}^2$ at time t and has a phase $\theta_i(t) \in [-\pi, \pi]$. The distance between two entities i and j is $d_{ij} := \|\boldsymbol{x}_j - \boldsymbol{x}_i\|$, and their phase difference is $\theta_{ij} := \theta_j - \theta_i$. The unit vector is $\boldsymbol{e}_{ij} := \frac{1}{d_{ij}} (\boldsymbol{x}_j - \boldsymbol{x}_i)$. The x and y-components of a vector $\boldsymbol{e}$ are written e_x and e_y.

The entities influence each other using a swarmalator model. The original model [1] uses attraction and repulsion kernels for swarming and synchronization, which we generalize by introducing exponents to these kernels. The system is then governed by:

$$\begin{aligned} \dot{\boldsymbol{x}}_i &= \frac{1}{N} \sum_{j \neq i}^{N} \boldsymbol{e}_{ij}\, d_{ij}^{\alpha} \left(1 + J \cos \theta_{ij}\right) - \boldsymbol{e}_{ij}\, d_{ij}^{\beta} \\ \dot{\theta}_i &= \frac{K}{N} \sum_{j \neq i}^{N} d_{ij}^{\gamma} \sin \theta_{ij} \end{aligned} \tag{1}$$

with two coupling parameters J and K, and the introduced kernel exponents $\alpha, \beta, \gamma > -2$. The equation for $\dot{\boldsymbol{x}}_i$ describes the movement of entity i in the two-dimensional

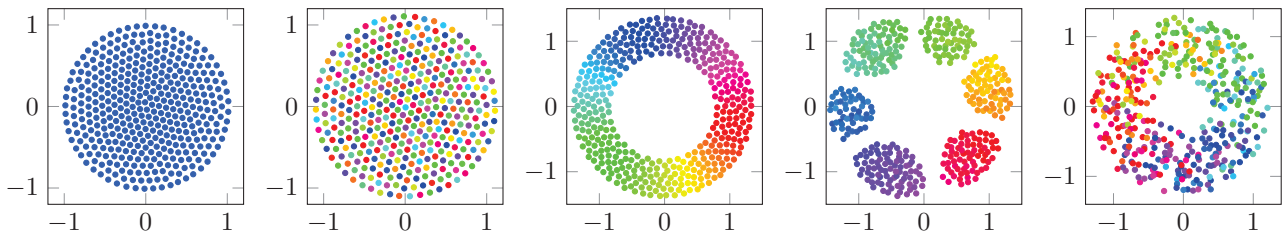

(a) *Static sync* (b) *Static async* (c) *Static phase wave* (d) *Splintered phase wave* (e) *Active phase wave*

Figure 1. Swarmalator patterns for $N = 400$ entities, parameters $\alpha = 0$ and $\beta = -1$ at time $t = 3{,}000$, starting with random positions and equidistant phases within the interval $[-\pi, \pi]$ (as in [1]).

979-8-3503-3744-0/23/$31.00 ©2023 IEEE
DOI 10.1109/ACSOS58161.2023.00034

space including its attraction to and repulsion from other entities. The parameter J controls the impact of phase synchrony on swarming, i.e., whether entities with similar phases attract ($J > 0$) or repel ($J < 0$) each other. The parameter K controls the influence of proximity on synchronization. These parameters determine the pattern type that results after some time. As shown in Fig. 1, we get: *static sync* ($J=0.1$, $K=1$), *static async* ($J=0.1$, $K=-1$), *static phase wave* ($J=1$, $K=0$), *splintered phase wave* ($J=1$, $K=-0.1$), and *active phase wave* ($J=1$, $K=-0.75$) [1]. Choosing $\alpha=0$ and $\beta=\gamma=-1$ gives the original model, and $\alpha=1$ and $\beta=\gamma=-1$ yields the linear kernel from the appendix of [1], which derives some properties of the patterns. All that follows is for $\gamma=-1$.

3. Derivation of Radii

All swarmalator patterns have a circular shape in their converged state, which can be characterized by an outer and an inner radius. The outer radius is $r_{\text{out}} := \max_{1\le i\le N} \|\boldsymbol{x}_i - \bar{\boldsymbol{x}}\|$, where $\bar{\boldsymbol{x}}$ is the mean position of all entities, i.e., the pattern center. Some patterns have a circular hole in their center; the radius of this hole is the inner radius $r_{\text{in}} := \min_{1\le i\le N} \|\boldsymbol{x}_i - \bar{\boldsymbol{x}}\|$. A normalized distance between i and j is $g_{ij} := d_{ij}/r_{\text{out}}$; we use a coordinate system with these normalized distances satisfying $\max_{i\neq j} g_{ij} = 2$.

In the converged state of the static patterns, the entities no longer move, so we have $\dot{\boldsymbol{x}}_i = 0$ in (1), which yields:

$$\underbrace{r_{\text{out}}^{\alpha} \sum_{j\neq i}^{N} \boldsymbol{e}_{ij}\, g_{ij}^{\alpha}\,(1 + J\cos\theta_{ij})}_{\text{Attraction } \mathcal{A}} = \underbrace{r_{\text{out}}^{\beta} \sum_{j\neq i}^{N} \boldsymbol{e}_{ij} g_{ij}^{\beta}}_{\text{Repulsion } \mathcal{R}} \quad . \tag{2}$$

Without loss of generality, the origin of the coordinate system is positioned in a way that the pattern center is at $\bar{\boldsymbol{x}} = (x, y) = (1, 0)$ and a swarmalator is present at the origin. This entity lies exactly on the perimeter of the pattern (see Fig. 2a). Based on this, we derive an expression for the length l_{O1} as a function of the angle ϕ. Elementary geometry gives $\theta = 2\phi$ and $l_{O1}(\phi) = \frac{\sin(2\phi)}{\sin\phi}$. Due to symmetry, the entity at the origin experiences zero net attraction and zero net repulsion into the y-direction, i.e., $\sum_{j\neq i}^{N} e_{ij_y}\, g_{ij}^{\alpha} = 0$ and $\sum_{j\neq i}^{N} e_{ij_y}\, g_{ij}^{\beta} = 0$, from which follows $r_{\text{out}}^{\alpha} \sum_{j\neq i}^{N} e_{ij_x} g_{ij}^{\alpha}\,(1 + J\cos\theta_{ij}) = r_{\text{out}}^{\beta} \sum_{j\neq i}^{N} e_{ij_x} g_{ij}^{\beta}$.

Next, we consider the limiting case $N \to \infty$ and rewrite the sums as integrals using polar coordinates (r, ϕ), hence substituting $e_{ij_x} = \cos\phi$ and $g_{ij} = r$, which yields

$$\text{Attraction} = \int_{-\frac{\pi}{2}}^{\frac{\pi}{2}} \cos\phi \int_0^{l_{O1}(\phi)} (1 + J\cos\theta_{ij}) r^{1+\alpha}\, \mathrm{d}r\, \mathrm{d}\phi \tag{3}$$

$$\text{Repulsion} = \int_{-\frac{\pi}{2}}^{\frac{\pi}{2}} \cos\phi \int_0^{l_{O1}(\phi)} r^{1+\beta}\, \mathrm{d}r\, \mathrm{d}\phi \quad \text{with} \tag{4}$$

$$r_{\text{out}}^{\alpha-\beta} = \frac{\text{Repulsion}}{\text{Attraction}}\,. \tag{5}$$

Static Sync. In static sync patterns, all phases are equal, which means that $J\cos\theta_{ij} = J\ \forall(i,j)$. For $\alpha = 0$ and $\beta = -1$, as in the original model [1], we get

$$r_{\text{out}} = \frac{\int_{-\frac{\pi}{2}}^{\frac{\pi}{2}} \cos\phi \frac{\sin(2\phi)}{\sin\phi}\, \mathrm{d}\phi}{(1+J)\frac{1}{2}\int_{-\frac{\pi}{2}}^{\frac{\pi}{2}} \cos\phi \frac{\sin^2(2\phi)}{\sin^2\phi}\, \mathrm{d}\phi} = \frac{3\pi}{8(1+J)}\,. \tag{6}$$

For $J = 0.1$, this results in $r_{\text{out}} \approx 1.071$. This value is close to the median value obtained from simulations done with finite N. For example, we get $r_{\text{out}} \approx 1.005$ for $N = 400$.

For a linear attraction kernel with $\alpha = 1$ and $\beta = -1$:

$$r_{\text{out}}^2 = \frac{\int_{-\frac{\pi}{2}}^{\frac{\pi}{2}} \cos\phi \frac{\sin(2\phi)}{\sin\phi}\, \mathrm{d}\phi}{(1+J)\frac{1}{3}\int_{-\frac{\pi}{2}}^{\frac{\pi}{2}} \cos\phi \frac{\sin^3(2\phi)}{\sin^3\phi}\, \mathrm{d}\phi} = \frac{1}{1+J}\,, \tag{7}$$

yielding $r_{\text{out}} = (1+J)^{-\frac{1}{2}}$, which corresponds to [1, (46)].

Static Async. For a small environment around a swarmalator at a position $\boldsymbol{x}_i$, there are infinitely many swarmalators each at a position $\boldsymbol{x}_j$ for which the distance is smaller than $\|\boldsymbol{x}_i - \boldsymbol{x}_j\| < \rho$ that have uniformly distributed phases. Thus, we get $\cos\theta_{ij} = \int_0^{2\pi} \cos\theta\, \mathrm{d}\theta = 0$. Equation (5) yields:

$$r_{\text{out}}^{\alpha-\beta} = \frac{\int_{-\frac{\pi}{2}}^{\frac{\pi}{2}} \cos\phi \int_0^{l_{O1}(\phi)} r^{1+\beta}\, \mathrm{d}r\, \mathrm{d}\phi}{\int_{-\frac{\pi}{2}}^{\frac{\pi}{2}} \cos\phi \int_0^{l_{O1}(\phi)} r^{1+\alpha}\, \mathrm{d}r\, \mathrm{d}\phi}. \tag{8}$$

For $\alpha = 0$ and $\beta = -1$, we get

$$r_{\text{out}} = \frac{\int_{-\frac{\pi}{2}}^{\frac{\pi}{2}} \cos\phi \frac{\sin(2\phi)}{\sin\phi}\, \mathrm{d}\phi}{\frac{1}{2}\int_{-\frac{\pi}{2}}^{\frac{\pi}{2}} \cos\phi \frac{\sin^2(2\phi)}{\sin^2\phi}\, \mathrm{d}\phi} = \frac{3\pi}{8} \approx 1.178 \tag{9}$$

This result is close to the median value of simulations, where we have $r_{\text{out}} \approx 1.106$ for $N = 400$.

A linear attraction kernel $\alpha = 1$ and $\beta = -1$ gives

$$r_{\text{out}}^2 = \frac{\int_{-\frac{\pi}{2}}^{\frac{\pi}{2}} \cos\phi \frac{\sin(2\phi)}{\sin\phi}\, \mathrm{d}\phi}{\frac{1}{3}\int_{-\frac{\pi}{2}}^{\frac{\pi}{2}} \cos\phi \frac{\sin^3(2\phi)}{\sin^3\phi}\, \mathrm{d}\phi} = 1\,, \tag{10}$$

which is the same as [1, (40)].

Static Phase Wave. The static phase wave pattern has an inner and an outer radius. Let r_r be the relative inner radius if the outer radius is normalized to 1. We define l_{O2} as the distance between the origin and the furthest part of the inner circle on a line with angle ϕ as in Fig. 2b. This yields

$$l_{O2}(\phi) = r_r \frac{\sin\left(\phi + \arcsin\frac{\sin\phi}{r_r}\right)}{\sin\phi} \tag{11}$$

for $\|\phi\| \le \arcsin r_r$. We set $l_{O2} = 0$ for $|\phi| > \arcsin r_r$, since the line is not intersecting with the inner circle. Next, we define l_{O3} as the distance between the origin and the closest point where the inner circle crosses the line with angle ϕ, as shown in Fig. 2c:

$$l_{O3}(\phi) = r_r \frac{\sin\left(\phi - \arcsin\frac{\sin\phi}{r_r} + \pi\right)}{\sin\phi} \tag{12}$$

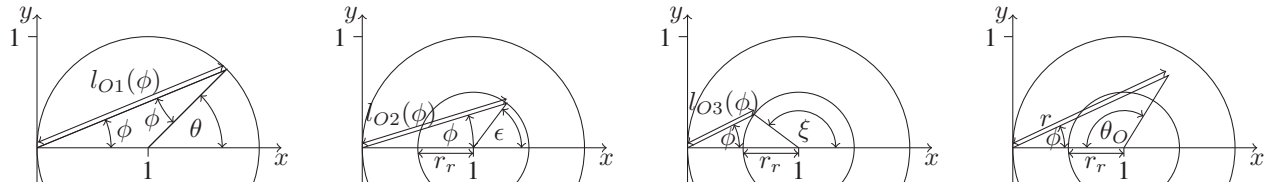

(a) Calculating the length $l_{O1}(\phi)$. (b) Calculating the length $l_{O2}(\phi)$. (c) Calculating the length $l_{O3}(\phi)$. (d) Calculating the phase θ_O.

Figure 2. Derivation of $l_{O1}(\phi)$, $l_{O2}(\phi)$, $l_{O3}(\phi)$, and θ_O.

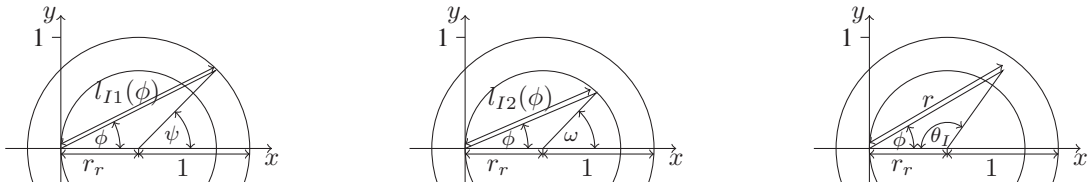

(a) Calculating the length $l_{I1}(\phi)$. (b) Calculating the length $l_{I2}(\phi)$. (c) Calculating the phase θ_I.

Figure 3. Derivation of $l_{I1}(\phi)$, $l_{I2}(\phi)$, and θ_I.

for $\|\phi\| \leq \arcsin r_r$, or $l_{O3} = 0$ for other values of ϕ. Furthermore, we calculate the phase θ_O as a function of the angle ϕ and the distance r from the origin as is shown in Fig. 2d, which leads to $\theta_O = \arctan \frac{\sin\phi}{\frac{1}{r}-\cos\phi}$. For $\cos\phi > \frac{1}{r}$, we need to further adjust the formula by subtracting $\pi \operatorname{sign}\left(\arctan \frac{\sin\phi}{\frac{1}{r}-\cos\phi}\right)$.

This results in

$$\mathcal{R}_O = \int_{-\frac{\pi}{2}}^{\frac{\pi}{2}} \cos\phi \left(\int_0^{l_{O3}(\phi)} r^{1+\beta}\,\mathrm{d}r + \int_{l_{O2}(\phi)}^{l_{O1}(\phi)} r^{1+\beta}\,\mathrm{d}r \right) \mathrm{d}\phi, \tag{13}$$

$$\mathcal{A}_O = \int_{-\frac{\pi}{2}}^{\frac{\pi}{2}} \cos\phi \left(\int_0^{l_{O3}(\phi)} (1 + J\cos(\theta_O)) r^{1+\alpha}\,\mathrm{d}r + \int_{l_{O2}(\phi)}^{l_{O1}(\phi)} (1 + J\cos(\theta_O)) r^{1+\alpha}\,\mathrm{d}r \right) \mathrm{d}\phi. \tag{14}$$

Since there are two unknown variables r_{out} and r_r, we need an additional equation to calculate numerical solutions. Thus, we shift the origin of the coordinate system by r_r to the right such that the inner circle passes the origin.

We define $l_{I1}(\phi)$ to be the length from the new origin to the perimeter of the swarm, as in Fig. 3a, which is

$$l_{I1}(\phi) = \frac{\sin\left(\phi + \arcsin\left(r_r \sin\phi\right)\right)}{\sin\phi}\,. \tag{15}$$

Next, we calculate the length $l_{I2}(\phi)$ from the origin to the inner circle along a line with angle ϕ as shown in Fig. 3b:

$$l_{I2}(\phi) = r_r \frac{\sin(2\phi)}{\sin\phi} \tag{16}$$

for $\|\phi\| \leq \frac{\pi}{2}$ and $l_{I2} = 0$ for ϕ not in this range. Finally, we calculate the phase θ_I as a function of the angle ϕ and the distance r as in Fig. 3c, resulting in $\theta_I = \arctan \frac{\sin\phi}{\frac{r_r}{r}-\cos\phi}$.

For $\cos\phi > \frac{r_r}{r}$, we need to further adjust the equation by subtracting $\pi \operatorname{sign}(\arctan \frac{\sin\phi}{\frac{r_r}{r}-\cos\phi})$. This gives

$$\mathcal{R}_I = \int_{-\pi}^{\pi} \cos\phi \int_{l_{I2}(\phi)}^{l_{I1}(\phi)} r^{1+\beta}\,\mathrm{d}r\,\mathrm{d}\phi, \tag{17}$$

$$\mathcal{A}_I = \int_{-\pi}^{\pi} \cos\phi \int_{l_{I2}(\phi)}^{l_{I1}(\phi)} (1 + J\cos(\theta_I)) r^{1+\alpha}\mathrm{d}r\,\mathrm{d}\phi\,. \tag{18}$$

We can solve for r_r and in turn calculate r_{out}. For all values of $\beta > -2$, (17) evaluates to

$$\mathcal{R}_I = \int_{-\pi}^{\pi} \cos\phi \int_{l_{I2}(\phi)}^{l_{I1}(\phi)} r^{1+\beta}\,\mathrm{d}r\,\mathrm{d}\phi = 0. \tag{19}$$

Since r_{out} and r_r are both strictly positive, it follows

$$\mathcal{A}_I = \int_{-\pi}^{\pi} \cos\phi \int_{l_{I2}(\phi)}^{l_{I1}(\phi)} (1 + J\cos(\theta_I)) r^{1+\alpha}\,\mathrm{d}r\,\mathrm{d}\phi = 0. \tag{20}$$

Solving this equation numerically for $\alpha = 0$, $\beta = -1$, and $J = 1$ gives $r_r \approx 0.5439$. Using (5) and the value calculated for r_r we get $r_{\text{out}} \approx 1.4076$. These numbers are close to the median value of the simulations that are $\hat{r}_o \approx 1.3721$ for $N = 400$. Numerically solving the equation for $\alpha = 1$, $\beta = -1$, and $J = 1$ leads to $r_r \approx 0.366$. Using (5) and the value calculated for r_r we get $r_{\text{out}} \approx 1.25593$. Again, these numbers are close to results in [1, (60)–(62)], where for a $J = 1$ we get $r_{\text{out}} \approx 1.26645$.

We use a similar approach for r_{in}. Here, we do not use relative coordinates but assume that r_{out} is known. The coordinate system is shifted such that the inner circle with radius r_{in} crosses the origin. This placement is similar to the one shown in Fig. 3 with the difference that the outer radius not is not necessarily 1.

Similar to the derivations shown before, we calculate the distances $l_{R1}(\phi)$ and $l_{R2}(\phi)$ from the origin to the outer circle and to the inner circle, respectively, yielding

$$l_{R1}(\phi) = r_{\text{out}} \frac{\sin\left(\phi + \arcsin(\frac{r_{\text{in}}}{r_{\text{out}}} \sin\phi)\right)}{\sin\phi} \tag{21}$$

$$l_{R2}(\phi) = r_{\text{in}} \frac{\sin(2\phi)}{\sin\phi} \tag{22}$$

for $\|\phi\| > \frac{\pi}{2}$, $l_{R2}(\phi) = 0$. For the phase θ_R, we get $\theta_R = \arctan \frac{\sin\phi}{\frac{r_{\text{in}}}{r} - \cos\phi}$.

For $\cos\phi > \frac{r_{\text{in}}}{r}$, we need to adjust the equation by subtracting $\pi \operatorname{sign}(\arctan \frac{\sin\phi}{\frac{r_{\text{in}}}{r} - \cos\phi})$.

We solve for r_{in}. Similar to (20), the repulsion vanishes:

$$\mathcal{R}_R = \int_{-\pi}^{\pi} \cos\phi \int_{l_{R2}(\phi)}^{l_{R1}(\phi)} r^{1+\beta} \,\mathrm{d}r \,\mathrm{d}\phi = 0\,. \tag{23}$$

Therefore, we can solve for r_{in} based on

$$\mathcal{A}_R = \int_{-\pi}^{\pi} \cos\phi \int_{l_{R2}(\phi)}^{l_{R1}(\phi)} (1 + J\cos\theta_R) r^{1+\alpha} \,\mathrm{d}r \,\mathrm{d}\phi = 0\,. \tag{24}$$

Solving the equation numerically using $\alpha = 0$, $\beta = -1$, and $J = 1$ yields $r_{\text{in}} \approx 0.7655$, which is about the median value from simulations, which is $r_{\text{in}} \approx 0.7995$ for $N = 400$. For $\alpha = 1$, $\beta = -1$, and $J = 1$ we get $r_{\text{in}} \approx 0.4597$ which is close to $r_{\text{in}} \approx 0.4768$ given in [1, (60)–(62)].

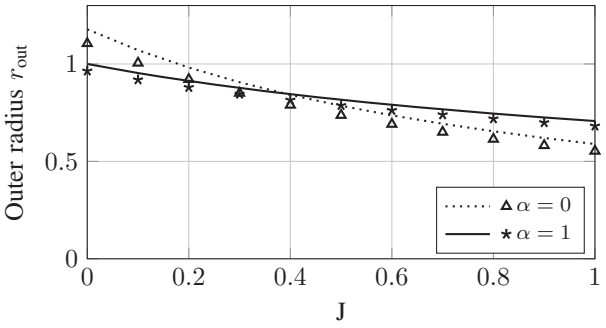

(a) Outer radius r_{out} over J with $\beta = -1$.

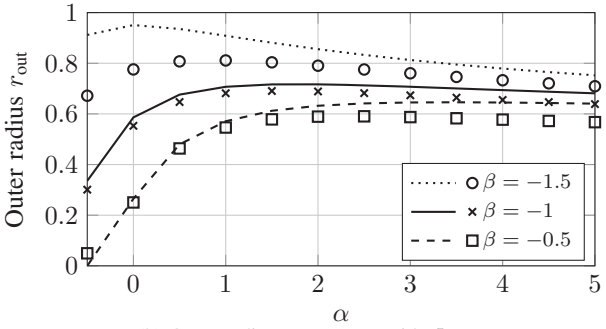

(b) Outer radius r_{out} over α with $J = 1$.

Figure 4. Static sync: Outer radius r_{out} with parameter $K = 1$. Lines are analytical results ($N \to \infty$); marks are simulation results ($N = 400$).

4. Numerical Evaluation

We now study how the pattern radii depend on α, β, and J. Our expressions for the asymptotic case are compared to simulations with a finite number of N entities. If not mentioned otherwise, we simulate $N = 400$ swarmalators. Each simulation run starts by placing the entities on a square grid of size 2×2. For the *static phase wave*, the phases are initialized with equidistantly distributed values $\theta_i = 2\pi(i-1)/N - \pi$, which leads to a regular pattern. For the other patterns, the phases are assigned randomly from a uniform distribution on $[-\pi, \pi]$. Simulations use Euler's method [7], which is a discrete time step approach for numerically solving differential equations of first order. In each step t, the values of the derivatives $\dot{\boldsymbol{x}}$ and $\dot{\theta}$ are calculated, and then applied to update the current state by $\boldsymbol{x}(t+1) = \boldsymbol{x}(t) + \dot{\boldsymbol{x}}(t)\Delta t$ and $\theta(t+1) = \theta(t) + \dot{\theta}(t)\Delta t$ with step size Δt. Simulations are performed with $\Delta t = 0.1$ for 3,000 time units (30,000 steps), and all plotted data points are averaged over 30 simulation runs. We keep $\alpha, \beta > -2$ as otherwise no stable pattern can form, and $\beta < 0$ to ensure repulsion acts locally and degrades for increasing distance.

4.1. Impact of Model Parameters

Static Sync. Fig. 4a shows the radius of the *static sync* pattern over J for $\alpha = 0$ and 1. The analytical results (line) always yield a slightly larger radius than the simulations (marks). This is because the radius increases with N in this pattern (see later in Fig. 9a), hence the assumption $N \to \infty$ leads to a larger radius than $N = 400$. In all cases, the radius decreases with increasing J and approaches zero in the limit $J \to \infty$. The limit $\beta \to \alpha-$ yields $r_{\text{out}} = 0$ for $J > 0$ and $\alpha > -2$.

Fig. 4b shows the radius over α for fixed J. Again, the equations always give a larger radius than the simulation. The patterns are less stable for some combinations of α and β (e.g., $\alpha = 0, \beta = -1.5$). Here, Δt must be reduced to reliably converge to the static sync pattern. An increase of β typically leads to a smaller radius, since higher β implies weaker repulsion. The dependence on α is not as straightforward: For $\alpha < 0$, the radius increases with α, as a higher α leads to a weaker attraction. For $\alpha > 0$, the radius is almost independent of α for $\beta \geq -1$, but it even decreases with α for $\beta = -1.5$ (where far-away entities with a distance above 1 are important for pattern formation).

Static Async. As shown in Fig. 5a, the choice of J in the *static async* pattern has no impact on the radius. However, if J is above a certain threshold, there is a soft transition to the *active phase wave*. If a value close to the threshold is chosen, the patterns are neither clearly static async nor active phase wave. Instead, new patterns emerge like presented in Fig. 6. Since the active phase wave forms a hole in the center, the outer radius r_{out} increases. This threshold depends on α. For $\alpha = 1$, it corresponds to the threshold given in [1, Fig. 1].

The impact of α (and β) on the radius is shown in Fig. 5b. There is a clear trend: For increasing α, the radius

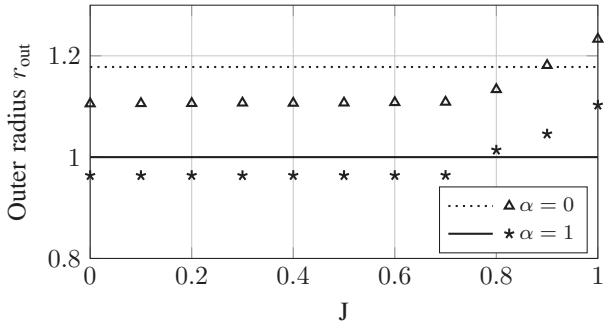

(a) Outer radius r_{out} over J with $\beta = -1$.

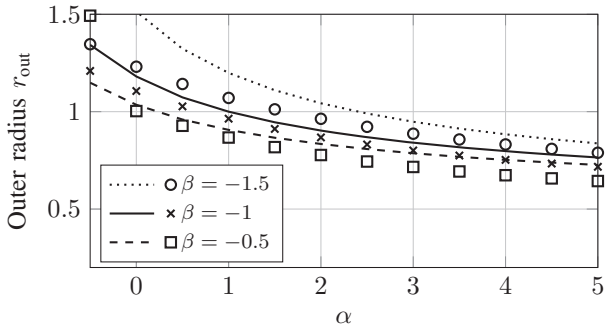

(b) Outer radius r_{out} over α with $J = 0.1$.

Figure 5. Static async: Outer radius r_{out} with parameter $K = -1$. Lines are analytical results ($N \to \infty$); marks are simulation results ($N = 400$).

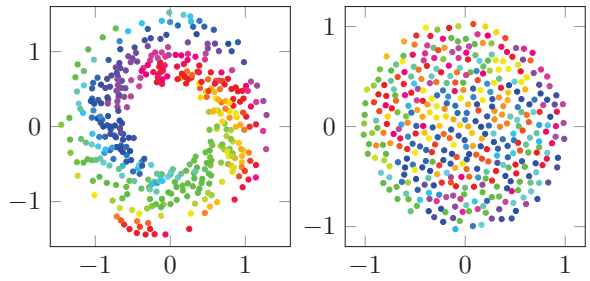

(a) *Milky way* (b) *Clustered static async*

Figure 6. Patterns between *static async* and *active phase wave* with $J = 1$ and $K = -1$. The *milky way* arises for $\alpha = -0.5$ and $\beta = -1$, the *clustered static async* for $\alpha = 2$ and $\beta = -1.5$. $N = 400$ and $t = 3000$

decreases. Here, the phase difference θ_{ij} plays an important role: Similar phases that lead to stronger attraction tend to be at a larger distance. Since high α increases the range of attraction, the overall attraction increases. The radius increases with less negative β since repulsion decreases.

Static Phase Wave. Results for the *static phase wave* are shown in Figs. 7 and 8. Both inner and outer radius increase with J for the given parameters (Figs. a). Again, simulations yield slightly smaller radii than the asymptotic equations. Results from [1, (60)–(62)] have an exact match for the outer radius and a good fit for the inner one with some slight deviations for J close to 1. Both radii diverge to infinity for

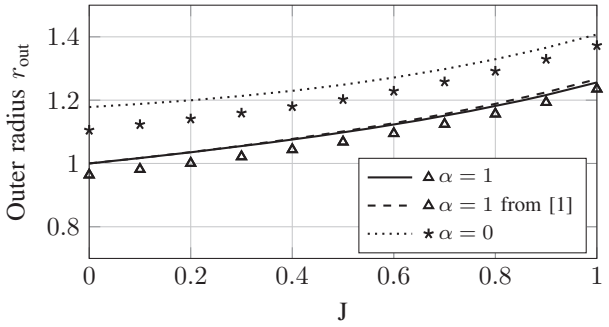

(a) Outer radius r_{out} over J with $\beta = -1$.

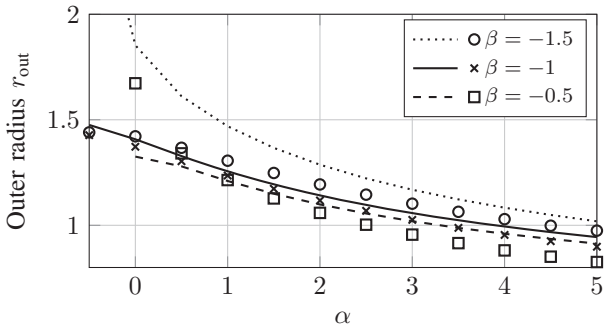

(b) Outer radius r_{out} over α with $J = 1$.

Figure 7. Static phase wave: Outer radius r_{out} with parameter $K = 0$. Lines are analytical results ($N \to \infty$); marks are simulation results ($N = 400$).

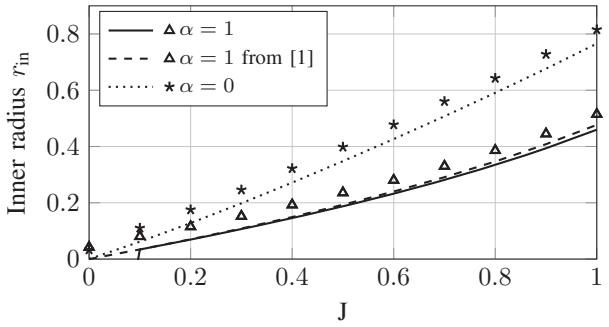

(a) Inner radius r_{in} over J with $\beta = -1$.

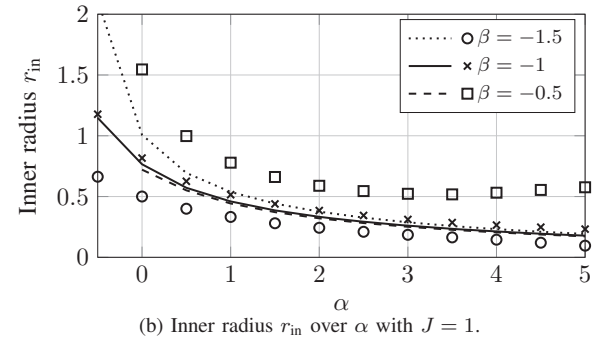

(b) Inner radius r_{in} over α with $J = 1$.

Figure 8. Static phase wave: Inner radius r_{in} with parameter $K = 0$. Lines are analytical results ($N \to \infty$); marks are simulation results ($N = 400$).

$J \to 2-$; no stable pattern can be formed for $J \geq 2$.

Next, we plot the radii for different α and β (Figs. b). Both radii decrease with increasing α. Higher β-values tend to give a smaller outer radius but show no clear trend for the inner one. Moreover, for smaller values of α and $\beta \neq -1$, the radius tends to deviate from the calculation more and more, as these patterns tend to be more unstable and converge to malformed shapes. For the inner radius, the data matches well if $\beta = -1$, but the order of traces is inverted for different β: the equation gives a smaller inner radius for $\beta = -0.5$, but a larger inner radius for $\beta = -1.5$ as compared to simulations. Further investigation is needed to obtain a deeper understanding of this phenomenon.

4.2. Impact of Number of Entities

Finally, we study the pattern radii as a function of N for $\alpha = 0$ and $\beta = -1$. For all patterns, the phases are assigned randomly using a uniform distribution. Simulations are performed 30 times and the median is taken. The results in Fig. 9 indicate that there is a strong impact of N on the radii for $N < 100$, whereas the results become less variant for higher N. However, even at around $N = 400$ the radii still change, which contributes to the difference to asymptotic results. For static sync and async, there is a trend toward larger outer radii for increasing N; in the static phase wave, the trend is inverted.

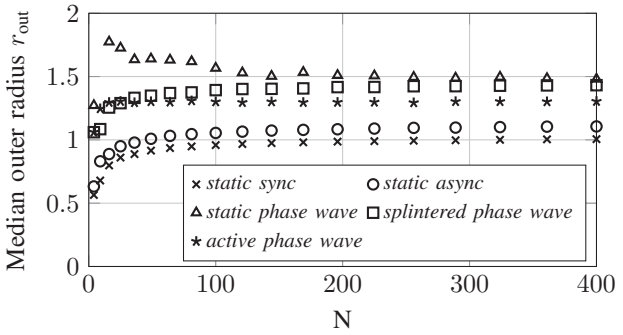

(a) The median outer radius r_{out}.

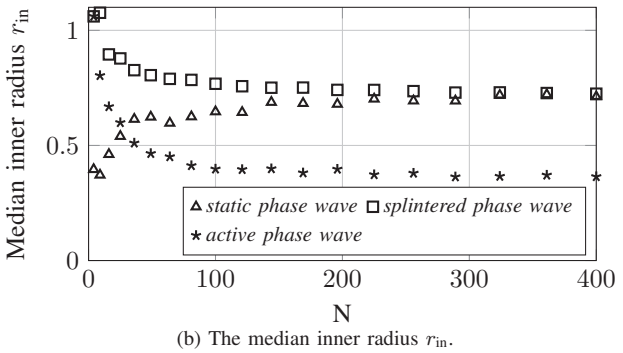

(b) The median inner radius r_{in}.

Figure 9. Simulation results of the median radii of *static phase wave, splintered phase wave*, and *active phase wave* with $\alpha = 0$ and $\beta = -1$.

5. Conclusions and Outlook

We derived and analyzed the size of static swarmalator patterns with parameterized kernels in the asymptotic case of infinitely many entities and compared the results to simulations with a finite number of entities. This generalizes known results with a linear attraction kernel ($\alpha = 1$, $\beta = -1$) [1].

A priori knowledge of the pattern size could help to apply swarmalators in practice and parameterize them for specific applications. For example, swarms of robots can now form patterns of desired size in a self-organized way without the need to program the movement paths. This is useful if robots must arrange around a point of interest to perform joint sensing. The results might also be applicable to natural systems in which combinations of synchronization and swarming occur [8]. Open issues include the analysis of non-static and three-dimensional patterns as well as stability with respect to the kernel exponents.

Acknowledgments

This work was funded by the Austrian Science Fund (FWF), grant *Self-organizing synchronization with stochastic coupling* (P30012).

References

[1] K. P. O'Keeffe, H. Hong, and S. H. Strogatz, "Oscillators that sync and swarm," *Nature Communications*, vol. 8, no. 1, p. 1504, 2017.

[2] H. Hong, K. P. O'Keeffe, J. S. Lee, and H. Park, "Swarmalators with thermal noise," *Physical Review Research*, vol. 5, p. 023105, 2023.

[3] A. Barciś, M. Barciś, and C. Bettstetter, "Robots that sync and swarm: A proof of concept in ROS 2," in *Proc. IEEE Intern. Symp. on Multi-Robot and Multi-Agent Systems (MRS)*, pp. 98–104, 2019.

[4] K. P. O'Keeffe and C. Bettstetter, "A review of swarmalators and their potential in bio-inspired computing," in *Proc. SPIE Micro- and Nanotechnology Sensors, Syst., and Appl. XI*, vol. 10982, Apr. 2019.

[5] S. Ceron, K. P. O'Keeffe, and K. Petersen, "Diverse behaviors in non-uniform chiral and non-chiral swarmalators," *Nature Communications*, vol. 14, no. 940, 2023.

[6] C. Müller-Schloer and B. Sick, *Organic Computing*, ch. Controlled Emergence and Self-Organization, pp. 81–103. Springer, 2008.

[7] B. N. Biswas, S. Chatterjee, S. P. Mukherjee, and S. Pal, "A discussion on Euler method: A review," *Electronic J. of Mathematical Analysis and Applications*, vol. 1, no. 2, pp. 294–317, 2013.

[8] A. Quillen, A. Peshkov, E. Wright, and S. McGaffigan, "Metachronal waves in concentrations of swimming turbatrix aceti nematodes and an oscillator chain model for their coordinated motions," *Physical Review E*, vol. 104, no. 014412, 2021.